

LETTER TO THE EDITOR

Magnetic braking below the cataclysmic variable period gap and the observed dearth of period bouncers

Arnab Sarkar¹, Antonio C. Rodriguez², Sivan Ginzburg³, Lev Yungelson⁴ and Christopher A. Tout¹

¹ Institute of Astronomy, The Observatories, Madingley Road, Cambridge CB3 0HA, UK
e-mail: as3158@cam.ac.uk

² Department of Astronomy, California Institute of Technology, Pasadena, CA 91125, USA

³ Racah Institute of Physics, The Hebrew University, Jerusalem 91904, Israel

⁴ Institute of Astronomy of the Russian Academy of Sciences, 48 Pyatnitskaya Str., 119017 Moscow, Russia

Received xx; accepted xx

ABSTRACT

Context. Period bouncers are cataclysmic variables (CVs) that have evolved past their orbital period minimum. The strong disagreement between theory and observations of the relative fraction of period bouncers is a severe shortcoming in the understanding of CV evolution.

Aims. We test the implications of the hypothesis that magnetic braking (MB), which is suggested to be an additional angular momentum loss (AML) mechanism for CVs below the period gap ($P_{\text{orb}} \lesssim 120$ min), weakens around their period minimum.

Methods. We computed the evolution of CV donors below the period gap using the MESA code, assuming that the evolution of the system is driven by AML due to gravitational wave radiation (GWR) and MB. We parametrised the MB strength as $\text{AML}_{\text{MB}} = \kappa \text{AML}_{\text{GWR}}$. We computed two qualitatively different sets of models, one in which κ is a constant and another in which κ depends on stellar parameters in such a way that the value of κ decreases as the CV approaches the period minimum ($P_{\text{orb}} \approx 80$ min), beyond which $\kappa \approx 0$.

Results. We find that two crucial effects drive the latter set of models. (1) A decrease in κ as CVs approach the period minimum stalls their evolution so that they spend a long time in the observed period minimum spike ($80 \lesssim P_{\text{orb}}/\text{min} \lesssim 86$). Here, they become difficult to distinguish from pre-bounce systems in the spike. (2) A strong decrease in the mass-transfer rate makes them virtually undetectable as they evolve further. So, the CV stalls around the period minimum and then ‘disappears’. This reduces the number of detectable bouncers. Physical processes, such as dynamo action, white dwarf magnetism, and dead zones, may cause such a weakening of MB at short orbital periods.

Conclusions. The weakening MB formalism provides a possible solution to the problem of the dearth of detectable period bouncers in CV observational surveys.

Key words. binaries: close – stars: magnetic field — novae, cataclysmic variables — white dwarfs – stars: late-type – brown dwarfs

1. Introduction

One of the most important challenges in our understanding of the evolution of cataclysmic variables (CVs, Warner 2003) is period bouncers. These are CVs that, according to the theory of CV evolution, widen their orbital separation after reaching a minimum in their orbital period, P_{orb} , owing to an interplay between their mass-loss timescale, thermal timescale, and degeneracy (Paczynski & Sienkiewicz 1981). However, the predicted fraction of period bouncers (70% by Kolb 1993, 40% by Golliasch & Nelson 2015) is much greater than that inferred observationally (14% by Pala et al. 2020, a few percent by Inight et al. 2023b).

Pala et al. (2020) point out that current models of CV evolution (e.g. Knigge et al. 2011) possibly do not correctly describe their evolution.¹ An important ingredient governing the evolution of such CVs is magnetic braking (MB). It is well established

¹ We note that, currently, virtually all theoretical population studies of CVs treat AML by MB, following the law that extrapolates empirically derived time-dependence of rotational velocities of ≈ 10 km/s of single stars (Skumanich 1972) to components of CVs with rotation velocities of ≈ 100 km/s (Verbunt & Zwaan 1981; Rappaport et al. 1983).

now that there may be a mechanism of angular momentum loss (AML) operating below the period gap ($P_{\text{gap}}, 2 \lesssim P_{\text{orb}}/\text{hr} \lesssim 3$) in addition to AML by gravitational wave radiation (GWR). This is because the period minimum, $P_{\text{min}} \approx 70$ min, by a system evolved solely with AML_{GWR} (Kalomeni et al. 2016) disagrees with observations, which find that $P_{\text{min}} \approx 80$ min (Gänsicke et al. 2009). Knigge et al. (2011) suggested that the existence of an additional AML below the period gap that is stronger by a factor of 1.47 than the AML_{GWR} can reproduce the P_{min} of CV correctly. However, there is no evidence that AML in short-period CVs can be simply described by a scaling factor applied to AML_{GWR} or that this scaling factor remains constant throughout the evolution of these CVs. Changing the AML strength of CVs at short periods has strong implications not only on their evolution but also on their detectability. The latter strongly depends on the inferred mass-transfer rate of the system (Appendix C). The essence of our proposed solution to the dearth of observed period bouncers is that although period bouncers exist, they are either difficult to distinguish from pre-bouncers, or simply not detectable.

In Sect. 2, we describe our weakening MB paradigm and illustrate its results. In Sect. 3, we discuss the physical pro-

cesses that can weaken MB in short-period CVs. We conclude in Sect. 4.

2. The weakening magnetic braking paradigm

Here, we describe our approach to study the implications of an MB strength that weakens around the CV period minimum.

2.1. Binary evolution calculation

We computed the evolution of CVs starting from a detached system with a fully convective donor of mass $M_{2,i} = 0.2M_{\odot}$, a WD accretor of mass $M_{1,i} = M_{WD,i} = 0.8M_{\odot}$, and an initial period of $P_{orb,i} = 3.18$ hr using version r23.05.1 of MESA (Paxton et al. 2011, 2013, 2015, 2018, 2019; Jermyn et al. 2023). The system parameters were chosen such that $P_{orb,i}$ is the upper limit of P_{gap} and $M_{2,i}$ is the donor mass at P_{gap} reported by Knigge et al. (2011). All our results were obtained by modifying `jdots_multiplier` in `project_inlist` in the MESA code, which multiplies AML_{GWR} by the factor `jdots_multiplier`. We call this factor $1 + \kappa$. We defined κ as a parametrised estimate of the strength of AML_{MB} . This approach is similar to that of Knigge et al. (2011). However, here κ may also depend on stellar parameters (Sect. 2.2). We assume fully conservative mass transfer so that the only mechanisms of AML are GWR and MB.

We note importantly that no unique $M_{2,gap}$ exists for all CVs, as is known from observations and theoretical computations (e.g. Knigge et al. 2011 and Sarkar & Tout 2022). This is because for un-evolved CV donors, $M_{2,gap}$ and the lower end of the period gap, at which mass transfer resumes ($P_{gap,-}$), depend on M_1 and the MB strength above the period gap. If we assume that the initial strength of MB below the period gap depends on stellar parameters, $M_{2,gap}$ and $P_{gap,-}$ set the initial κ of our systems. In the next section, we choose how κ behaves as the CV evolves.

2.2. The method

We considered two qualitatively different sets of models, one in which κ is a constant throughout and another in which κ varies with stellar parameters. In the first set, we computed models evolved with $\kappa = 0, 4, \text{ and } 15$ (Fig. 1). The latter two κ s are purely ad hoc and were chosen to aid understanding of an MB that depends on stellar parameters, described later. The system with $\kappa = 0$ evolves solely with GWR and represents the minimum P_{orb} of a given M_2 . Systems such as polars (AM Her systems, Li et al. 1994), in which there is no MB, follow this track. In zero-age CVs with some degree of MB, $\kappa > 0$ initially. We plot in Fig. 1 CVs with donor masses and periods, estimated from superhump periods, assuming $M_1 = 0.75M_{\odot}$ by Knigge (2006, their Table 1).² There is quite a bit of scatter among these points and they do not seem to converge on a unique evolutionary track. This illustrates that varying strengths of MB likely operate below the period gap.³ However, studying the significance of this effect is beyond the scope of this Letter. The track with $\kappa = 15$ matches with the systems with the biggest P_{orb} for a given M_2 in the catalogue of Knigge (2006). So, hereinafter, we assume that

² These are pre-bounce CVs. The M_2 for post-bounce CVs was calculated differently (Sect. 2.3).

³ We note that the scatter of the systems in the catalogue of Knigge (2006) may be the result of other evolutionary processes which can alter the thermal timescale of the donor.

the tracks with $\kappa = 15$ and $\kappa = 0$ exhibit, respectively, the upper and lower limits of P_{orb} for a given M_2 .

The other set of tracks, in which κ varies with stellar parameters, illustrates the behaviour of the system when the strength of MB depends on stellar structure and changes as the donor evolves. We used the result of the strong- and weak-field dynamo for fully convective low-mass stars proposed by Morin et al. (2011) to model such an MB strength. They argued, based on spectropolarimetric observations by Morin et al. (2010), that two different magnetic field profiles exist in isolated fully convective stars with similar rotation rates and masses. The first is a strong and steady axial dipole field and the second is a weak, multi-polar non-axisymmetric field that is changing rapidly. Because donors in short-period CVs are fully convective, it is possible that a strong-field dynamo also operates in such CV donors in which it drives MB. So, we used the formula for the magnetic field given by Morin et al. (2011, their Eq. (2)) to define κ (for details on how they derive their magnetic field expression, we urge the reader to refer to their Sect. 4.2). Other physical mechanisms that may lead to a stellar-dependent κ are discussed in Sect. 3.

We defined a dimensionless quantity, B , as a proxy for the magnetic field as⁴

$$B = \frac{6 \text{ kG}}{19.5 \text{ kG}} \left(\frac{M_2}{M_{\odot}} \right)^{1/2} \left(\frac{R_2}{R_{\odot}} \right)^{-1} \left(\frac{L_2}{L_{\odot}} \right)^{1/6} \left(\frac{P_{orb}}{d} \right)^{-1/2}, \quad (1)$$

where R_2 and L_2 are the radius and the luminosity of the donor, respectively. We computed these using MESA. The last term in Eq. (2) of Morin et al. (2011) is $(P_{spin}/d)^{-1/2}$, where P_{spin} is the spin period of the M-dwarf. This becomes $(P_{orb}/d)^{-1/2}$ in our Eq. (1) because of tidal locking. The denominator 19.5 kG is the dipolar field at the time of the commencement of Roche lobe overflow (RLOF). This ensures that $B < 1$ throughout the evolution. We plot two tracks in which $\kappa = 15B^2$ and $\kappa = 15B^4$. The exponents are ad hoc but highlight the varying degrees of the dependence of MB strength on the magnetic field, and hence the stellar structure. They also lead to the system attaining P_{min} at 86 and 80 min, respectively (Fig. 1), which are the upper and lower limits of the observed period minimum spike reported by Gänsicke et al. (2009). The behaviour of B can be understood as follows. Because of RLOF and the fact that the donors are close to thermal equilibrium, R_2 , L_2 , and P_{orb} are functions of M_2 , and so $B \equiv B(M_2)$ and $P_{orb} \propto R_2^{3/2} M_2^{-1/2}$. For our donors, $L_2 \propto M_2^{\beta}$, in which $2 \lesssim \beta \lesssim 4$ depending on the mass-transfer rate. If we define $R_2 \propto M_2^{\alpha}$, we get $B \propto M_2^{3/4+\beta/6-7\alpha/4}$. We have $\alpha > 0$ pre-bounce and $\alpha \lesssim 0$ post-bounce. Choosing $\beta = 3$, $\alpha = 0.6$ pre-bounce and $\alpha = 0.3$ post-bounce (similar to eq. (16) of Knigge et al. 2011), we get $B \propto M_2^{0.2}$ pre-bounce and $B \propto M_2^{0.725}$ post-bounce. So, post-bounce B decreases strongly because of a change in the $M_2 - R_2$ relation of the donor. The evolution of B is shown in Fig. 1.

2.3. Results

We follow the evolution of the models with $\kappa = 15B^2$ and $\kappa = 15B^4$ in the $M_2 - P_{orb}$ plane. At $M_2 \approx 0.2M_{\odot}$, these systems are driven by strong MB so they follow the track with $\kappa = 15$.

⁴ There is an additional term $(\eta_{\odot}/\eta_{ref})^{1/2}$ in the expression of the magnetic field in Morin et al. (2011). Here $\eta_{ref} \equiv 10^{11} \text{ cm}^2 \text{ s}^{-1}$ is the magnetic diffusivity and η_{\odot} is the reference magnetic diffusivity. Studying how this term varies for our CVs is beyond the scope of this work. So we set $(\eta_{\odot}/\eta_{ref}) = 1$.

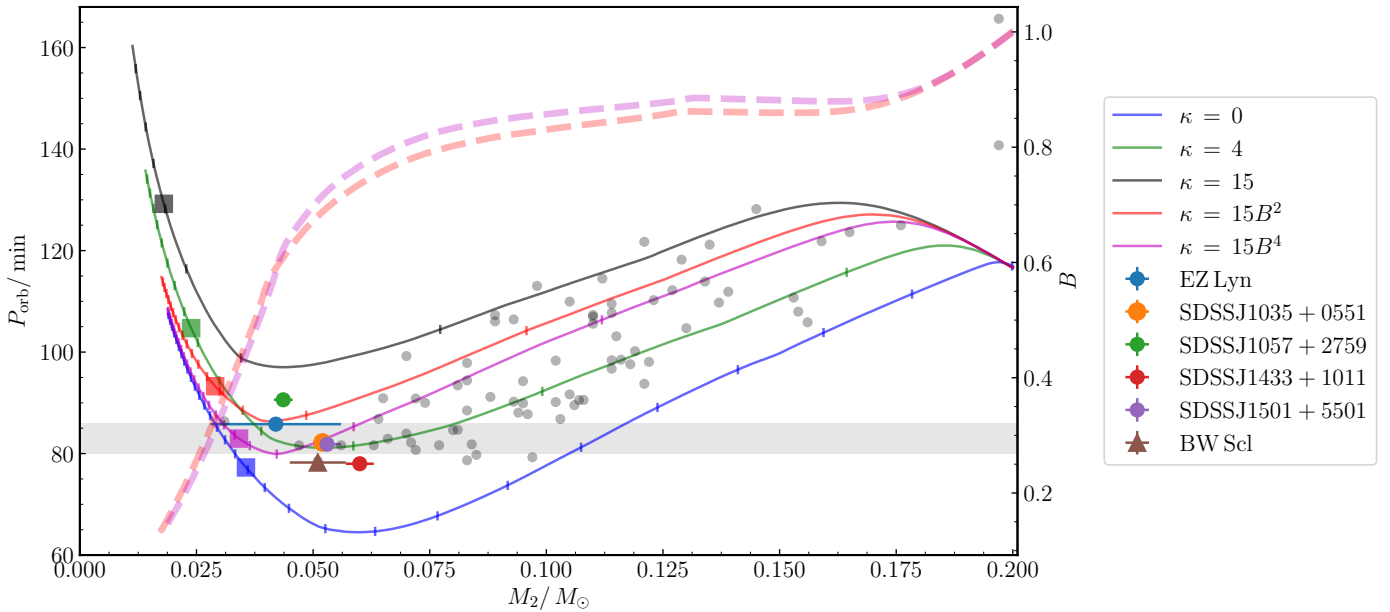


Fig. 1. Evolution of CVs below the period gap. The solid lines show the tracks on the $M_2 - P_{\text{orb}}$ plane (lower x- and left y-axis). The dashed tracks in the $M_2 - B$ plane (lower x- and right y-axis) show the evolution of B (Eq. (1)) for the models in which κ depends on stellar parameters. The ticks on each solid track denote timesteps of 300 Myr. The different colors correspond to different κ s. The grey points are CVs reported by Knigge (2006, their Table 1). We also plot observed period bouncer candidates from Table B.1. Eclipsing systems are plotted as circles, while non-eclipsing systems are plotted as triangles. The horizontal shaded region is the observed period minimum spike ($80 \leq P_{\text{orb}}/\text{min} \leq 86$) reported by Gänsicke et al. (2009). The squares of different colors show when the system has $\dot{M}_2 = 10^{-11} M_{\odot} \text{yr}^{-1}$. During further evolution, the system is presumably undetectable (see text).

However, B starts decreasing gradually at $M_2 \approx 0.125 M_{\odot}$ and substantially when $M_2 \lesssim 0.05 M_{\odot}$. This leads to the weakening of the MB strength. We note, importantly, that for all our models, the absolute value of AML decreases as the CV evolves (see Appendix A). So, the ‘weakening’ of MB is the additional weakening of the MB strength caused by B (Fig. A.1). The weakening of MB is such that the donor star always adjusts to it on its thermal timescale. The extent of the weakening depends on the exponent of B . Close to their respective P_{min} , MB becomes negligible. This can be understood with Eq. (1) — further evolution decreases M_2 and increases R_2 and, as a consequence, P_{orb} . These systems, now only driven by GWR, evolve further to converge to the $\kappa = 0$ track. This causes their evolution timescale to drastically increase around and beyond their P_{min} . Owing to their long evolutionary timescales, these systems stall in the period minimum spike and spend a lot of time there compared to systems evolved with a constant κ . Because the systems are clustered around the period minimum spike, here it is very difficult to distinguish between pre-bounce and post-bounce systems observationally (Pala et al. 2018). We highlight that the weakening MB models also reproduce the period minimum reported by Knigge et al. (2011) but that the M_2 at which P_{min} is attained is much smaller than the $0.069 M_{\odot}$ reported by Knigge et al. (2011). So, if MB weakens in near- P_{min} CVs, our models suggest that most of the period bouncer candidates in Fig. 1 are pre-bounce CVs.

At this stage the problem is far from over. Any MB strength below the period gap will only accelerate the evolution of short-period CVs towards their period minimum and drive more CVs to form period bouncers. This will lead to more period bouncers than are predicted solely using GWR (e.g. Kolb 1993, Goliasch & Nelson 2015), and thus exacerbate the classical problem of the dearth of observed period bouncers. For a detectable period bouncer we not only need $P_{\text{orb}} \geq P_{\text{min}}$ and $M_2 \leq M_2(P_{\text{min}})$, but

also $\dot{M}_2 > \dot{M}_{2,\text{detect}}$, where $\dot{M}_{2,\text{detect}}$ is the detection threshold in the mass-transfer rate, \dot{M}_2 .

All of our candidate bouncer CVs (Table B.1) have \dot{M}_2 (estimated by Eq. (C.1) using WD properties) about a few times $10^{-11} M_{\odot} \text{yr}^{-1}$ (also see Pala et al. 2022). So, we assume an optimistic detection threshold of $\dot{M}_2 = 10^{-11} M_{\odot} \text{yr}^{-1}$ such that any system below this limit is undetectable. The impact of such observational selection effects have been explored in the past (e.g. Pretorius et al. 2007, Inight et al. 2023a). This limit is likely to change with emerging data from optical and X-ray surveys, such as SDSS-V (Kollmeier et al. 2017) and SRG/eROSITA (Predehl et al. 2021; Sunyaev et al. 2021), respectively. The former has already led to the discovery of new period bouncer candidates, which are optically fainter than much of the population (Inight et al. 2023b). The latter is five to 15 times deeper than the last all-sky X-ray survey, potentially revealing systems with lower accretion rates; for instance, the bouncer candidate reported by Galiullin et al. (2024). In Appendix C, we discuss the effects of using \dot{M}_2 derived from X-ray luminosity and its limitations. Later in this section we also discuss the effect of changing $\dot{M}_{2,\text{detect}}$.

A complete picture of how the weakening of MB can reduce the number of detectable period bouncers is shown in Fig. 2. We chose $\dot{M}_{2,\text{detect}} = 10^{-11} M_{\odot} \text{yr}^{-1}$ (circles in each track), beyond which the system becomes undetectable. Although $\dot{M}_{2,\text{detect}}$ is model-independent, how a variable MB strength drives a system to reach this $\dot{M}_{2,\text{detect}}$ is model-dependent. In the $t - \dot{M}_2$ plot, it can be seen that the M_2 of the $k = 15B^4$ model attains $\dot{M}_{2,\text{detect}}$ earlier than that of the other two models. The time evolution of P_{orb} and M_2 is affected because of this. In the $t - P_{\text{orb}}$ plot, the $\kappa = 4$ model bounces at 80 min and becomes undetectable at 105 min at $t = 0.94$ Gyr. The $\kappa = 0$ model bounces at 65 min and becomes undetectable at 78 min at $t = 1.15$ Gyr. The $k = 15B^4$ model bounces at 80 min and becomes unde-

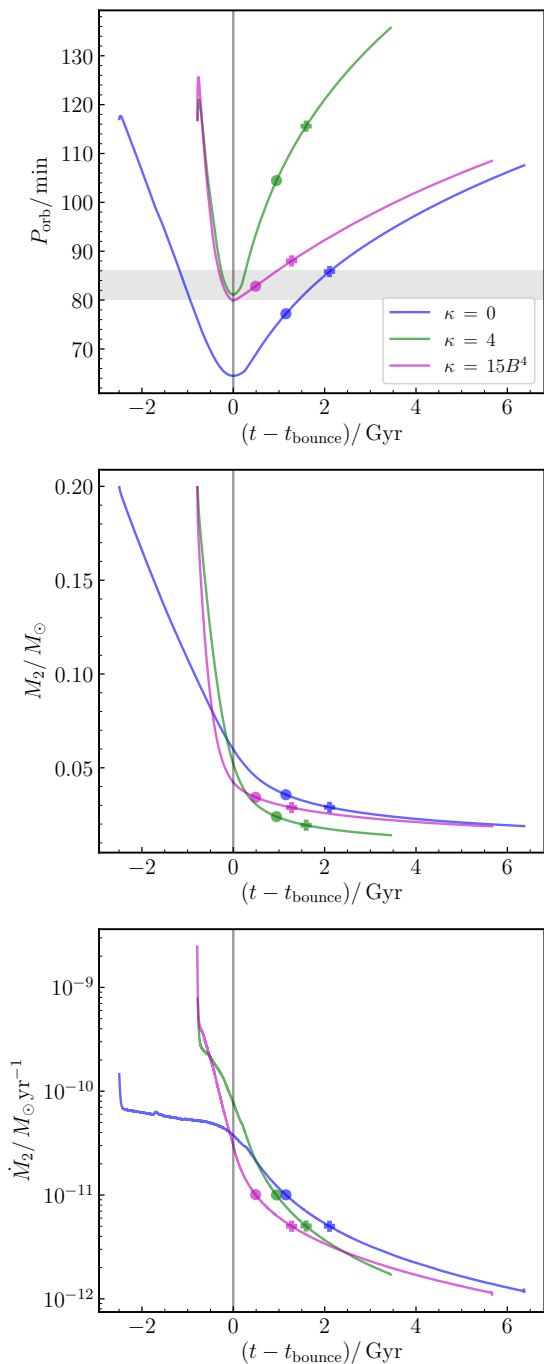


Fig. 2. Time evolution of P_{orb} , M_2 , and \dot{M}_2 for three choices of κ . The vertical black line in each subplot is the time at which the system attains its period minimum (t_{bounce}). The circles and pluses in each track mark detection thresholds of $\dot{M}_2 = 10^{-11} M_{\odot} \text{yr}^{-1}$ and $5 \times 10^{-12} M_{\odot} \text{yr}^{-1}$ (see text). The shaded region in the top subplot is the observed period minimum spike.

detectable at 83 min at $t = 0.48$ Gyr. So the weakening MB system becomes undetectable earlier and without much change in P_{orb} post-bounce (there is only about a 3 min difference between bounce and non-detection). The $\kappa = 4$ and $\kappa = 0$ models have a large difference between the P_{orb} in which they bounce and in which they become undetectable. The same is true in the $t - M_2$ plot. In the model with weakening MB, there is little change in its M_2 between bounce and non-detection, while the change is more significant for the $\kappa = 0$ and $\kappa = 4$ models. The results do

not change qualitatively if we take $\dot{M}_{2,\text{detect}} = 5 \times 10^{-12} M_{\odot} \text{yr}^{-1}$ (pluses in each track), the limit we expect from SRG/eROSITA (Galiullin et al. 2024). In other words, we conclude that the weakening of MB greatly slows down the evolution of the system, with lesser change in M_2 and P_{orb} , from the time it bounces to the time it becomes undetectable. However, we note that all our tracks asymptotically tend to $\dot{M}_2 = 10^{-12} M_{\odot} \text{yr}^{-1}$. So, our idea makes a strong testable prediction for finding many low-luminosity bouncers aggregated at $\dot{M}_2 \approx 10^{-12} M_{\odot} \text{yr}^{-1}$ in the upcoming surveys (e.g. Galiullin et al. 2024). A dearth of CVs at these \dot{M}_2 will easily falsify this theory, although finding such low \dot{M}_2 might be difficult (see Appendix C). The evolution of the models in the $\dot{M}_2 - P_{\text{orb}}$ plane is shown in Fig. C.1 and discussed in detail in Appendix C.

For $\dot{M}_{2,\text{detect}} = 10^{-11} M_{\odot} \text{yr}^{-1}$, our weakening MB model ($\kappa = 15B^4$) predicts a reduction in the time spent by a system as a detectable bouncer by a factor of 2.35 compared to the GWR model. Simply reducing the fraction of bouncers predicted by solely using GWR in Kolb (1993, about 70%) and Goliash & Nelson (2015, about 40%) by 2.35, we get equivalent fractions of detectable period bouncers of about 30% and 17%, respectively. We note that the estimates of Kolb (1993) and Goliash & Nelson (2015) are the fraction of all period bouncers. The detectable ones are a small subset of it. Additionally, a further reduction to match the observationally inferred estimates (e.g. Inight et al. 2023b) is possible because we show that detectable bouncers populate the period minimum spike that is also populated by pre-bounce CVs. Here, they are difficult to distinguish observationally (Pala et al. 2018).

We note that although Inight et al. (2023a,b) show that bouncers make up only a few percent of the total CV population, this population also consists of magnetic CVs, which follow a different evolution than non-magnetic CVs (Li et al. 1994). If we assume that bouncers remain non-magnetic throughout (although see Sect. 3.2), a better estimate of the fraction of bouncers amongst all non-magnetic short-period CVs can be obtained from the top panel of fig. 33 of Inight et al. (2023a). Here, we designate SU UMa systems as pre-bounce CVs and assume that most WZ Sge are bouncers. These assumptions, although crude, allow us to approximate that period bouncers make up roughly 30% of all non-magnetic CVs below the period gap in the SDSS I to IV catalogue.

We perform a direct comparison of our results with that of Inight et al. (2023a) using the distribution of the evolution time spent by our systems as a function of P_{orb} and \dot{M}_2 in Fig. 3. Because we make no claims on the nature of MB above the period gap, we assume that all our models follow identical evolution till the lower end of the period gap. So, the time spent by a system at a given P_{orb} and \dot{M}_2 interval below the gap is proportional to the number of systems in that interval. As was expected, it is seen that the intrinsic distribution of short-period non-magnetic CVs is dominated by bouncers. The intrinsic fraction of bouncers is about 74% for $\kappa = 0$, 82% for $\kappa = 4$, and 87% for $\kappa = 15B^4$. This was also expected, because in the $\kappa = 15B^4$ model we introduce a substantial MB at the beginning, which drives more CVs towards becoming bouncers.

Because the $\kappa = 4$ and $\kappa = 15B^4$ models have similar P_{min} , we analysed how their features may compare with observations. We calculated the number of bouncers that would have to become invisible below a certain \dot{M}_2 cut-off⁵ for our fraction of visible period bouncers to corroborate the 30% that we obtained from fig. 33 of Inight et al. (2023a). For $\kappa = 15B^4$,

⁵ These need not necessarily be our previous $\dot{M}_{2,\text{detect}}$.

the limit is $\dot{M}_2 \approx 1.2 \times 10^{-11} M_\odot \text{yr}^{-1}$, so that about 94% of the intrinsic bouncers become invisible. For $\kappa = 4$, the cut-off is $\dot{M}_2 \approx 3.2 \times 10^{-11} M_\odot \text{yr}^{-1}$, so that about 90% of the intrinsic bouncers become invisible. The factor of 2.7 between the \dot{M}_2 cut-off in the two models may not seem dramatic, so its significance needs to be emphasised. For an \dot{M}_2 cut-off of $\approx 1.2 \times 10^{-11} M_\odot \text{yr}^{-1}$, the fraction of bouncers in the $\kappa = 4$ model increases to about 50%, meaning that 20% of bouncers exist for $1.2 \times 10^{-11} \lesssim \dot{M}_2 / M_\odot \text{yr}^{-1} \lesssim 3.2 \times 10^{-11}$. In other words, for any detection cut-off in \dot{M}_2 , our weakening MB models will be more affected than the constant MB ones and corroborate observations better.

We note that there is no reason to suggest that our analyses with an ad hoc power of B in an expression of MB derived from the prescription of Morin et al. (2011) would provide a robust comparison with the detailed observational work of Inight et al. (2023a,b). In this work, we just show that for a given observational cut-off, the number of detectable bouncers reduces strongly if MB weakens post-period minimum. The strength of this reduction, in turn, depends on how strongly MB weakens. An extreme case of this is if post-minimum, MB weakens on a dynamical timescale. In such a case, the CV detaches, as is suggested by Inight et al. (2023a), and remains so for about a Gyr (see Fig. 2) till GWR resumes RLOF.

It is important to discuss our results in the context of certain population synthesis studies; for instance, Pretorius et al. (2007) and Belloni et al. (2020). They find, using MB from Verbunt & Zwaan (1981) and Rappaport et al. (1983) above the period gap, respectively, and no MB below the gap, that the intrinsic CV population cannot contain as large a fraction of short-period systems, specifically period bouncers, as is predicted by theory and that selection effects (such as our $\dot{M}_{2,\text{detect}}$ cut-off) cannot reconcile the predictions of CV evolution theory with observations. At first glance, these results seem to defeat the main idea in this paper, in which our claim that there is an MB strength about 15 times as strong as AML_{GWR} below the period gap exacerbates this apparent discrepancy. However, we note that the intrinsic populations constructed by Pretorius et al. (2007) and Belloni et al. (2020) entirely depend on their assumed MB strength above the period gap. There is evidence to suggest that a weaker MB possibly operates above the gap (Knigge et al. 2011). A weaker MB above the period gap lowers the birthrate of all CVs, which agrees with Pala et al. (2020), who find a lower space density of CVs. Fig. 2 of Knigge et al. (2011) illustrates that the AML strengths via MB in Verbunt & Zwaan (1981) and Rappaport et al. (1983) are about two orders of magnitude stronger than GWR above the period gap. So, no matter what strength of MB we choose below the gap, too many CVs have already been driven below the period gap by the strong MB above the gap and so a discrepancy between theory and observations is bound to arise. What causes the discrepancy between theoretical predictions and observations is not what one chooses as MB below the period gap but what one chooses as MB above the period gap. In other words, a modest initial MB strength of about $15\text{AML}_{\text{GWR}}$ below the period gap cannot undo the accumulation of CVs already dumped there by a strong MB above the gap. Because we make no claims about MB above the gap in this work, there is no reason for our idea to corroborate studies in which the theoretical CV population is entirely shaped by uncertain estimates of a strong MB above the period gap.

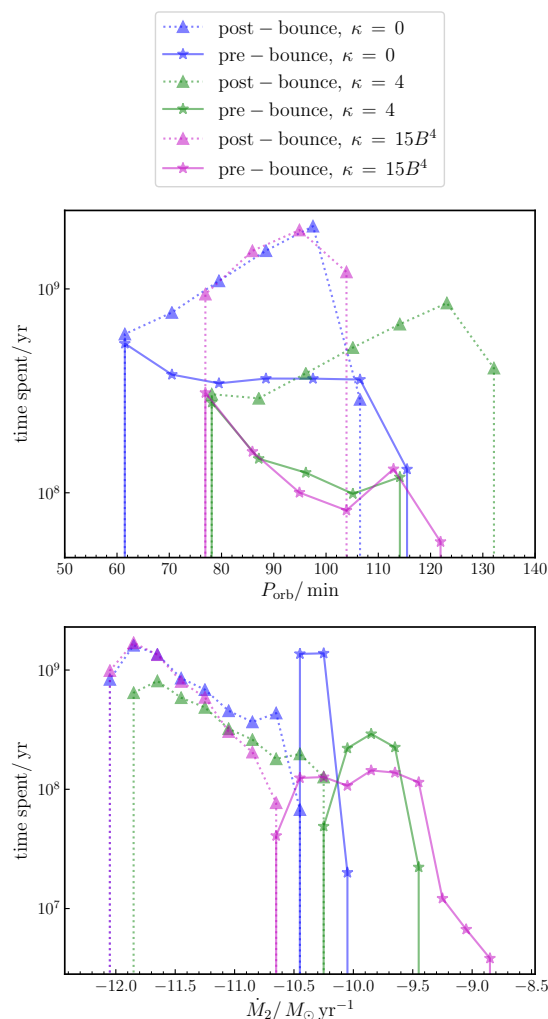


Fig. 3. Distributions of the evolution time spent at each increment of P_{orb} and \dot{M}_2 for three choices of κ . The stars denote pre-bouncers ($M_2 > M_2(P_{\text{orb}} = P_{\text{min}})$) and triangles denote post-bouncers. Top panel: Systems evolving from right to left as pre-bouncers (star symbols) and from left to right (triangles) post-bounce. Bottom panel: Systems evolving from right to left.

3. Physical processes driving the weakening of magnetic braking

We highlight a few physical processes that may cause the weakening of MB in short-period CVs. We note that this list is not exhaustive and that there can be additional mechanisms driving such a weakening.

3.1. Dynamo action in cool stars

In Sect. 2.2, we showed that if the strong-field dynamo proposed by Morin et al. (2011) operates in short-period CV donors, Eq. (1) causes B to reduce significantly for $M_2 \lesssim 0.07 M_\odot$. There is observational evidence to suggest that stars with $T_{\text{eff}} \lesssim 2200 \text{K}$ such as L-dwarfs have significantly lower chromospheric activity compared to M-dwarfs despite being rapid rotators (Mohanty & Basri 2003). This means that the magnetic field strength drops from fully convective M-dwarfs to brown dwarfs. In Sect. 2.2, we showed that this drop may be due to the change in the mass-radius relation of the star. The results of the α^2 dynamo model proposed by Chabrier & Küker (2006) have also shown, simi-

larly to Morin et al. (2011), that there is a transition in the magnetic field structure from a steady, large-scale field in late M-dwarfs to a toroidal, oscillatory one in brown dwarfs. In addition, the conductivity of the atmosphere of cool objects such as brown dwarfs decreases greatly, thereby hampering the formation of a hot corona that would drive stellar winds. The combined effect of weaker stellar winds and reduced magnetic field strength drives a weaker MB in brown dwarfs (Mohanty & Basri 2003; Chabrier & Küker 2006). In other words, if such a dynamo operates in short-period CV donors, MB reduces significantly as the donor enters the brown dwarf regime ($M_2 \lesssim 0.07M_\odot$).

3.2. White dwarf magnetism

Isern et al. (2017) suggest that cool WDs generate strong magnetic fields by a crystallization-driven dynamo. Schreiber et al. (2021) show that magnetic CVs can be explained by the rapid rotation and crystallization of the WD accretors, which can generate fields of several MG (Ginzburg et al. 2022). Schreiber et al. (2023) have recently proposed that such fields are generated in the accretor of short-period CVs post-period minimum. This field connects with that of the donor star, resulting in the detachment of period bouncers for several gigayears. They argue that this can lead to a reduction of about 60% in the number of observed bouncers.

We illustrate a variation in their analysis in which the CV may remain semi-detached. Schreiber et al. (2023) assume that the diffusion timescale of the magnetic field to the WD surface is 100 Myr (Fig. 3 of Ginzburg et al. 2022). However, recently Blatman & Ginzburg (2024) showed that the magnetic field on the WD surface gradually emerges on a gigayear timescale (their bottom right subplot in Fig. 1). By consistently taking into account phase separation, they find that the magnetic diffusion time is about 1 Gyr at the time of breakout and shortly afterwards (this also depends on the WD mass). The donor has a thermal timescale of around a few gigayears, depending on the mass-transfer rate. Since the thermal timescale of the donor is comparable to the diffusion timescale of the WD magnetic field, there is a possibility that the donor adjusts to the reduction in MB because of magnetic reconnection post-period minimum, while continually filling its Roche lobe. In such a case, the evolution will be similar to that presented in Sect. 2. However, such a weakening depends on the properties of the WD accretor, such as its mass and temperature, but is independent of the donor star transitioning from an M-dwarf to a brown dwarf. So, such systems would not necessarily experience an MB weakening at $M_2 \approx 0.07M_\odot$ but when the WD becomes magnetic (Schreiber et al. 2023).

3.3. Dead zones

The dead zone is the region around a spinning magnetised star in which the stellar wind is captured and forced to co-rotate along its magnetic field lines (Mestel & Spruit 1987). This leads to a reduction in wind mass loss and, as a consequence, the strength of MB. Dead zones were first studied by Mestel & Spruit (1987) who gave a simple description for isolated solar-like stars with different rotation rates. Subsequently, several groups have implemented the effects of dead zones in their calculations of MB torque in stellar spin-down (Réville et al. 2015; Garraffo et al. 2015). Because dead zones arise through the interplay of gravity, centrifugal force, and magnetism in the star, they should be at play in every system undergoing MB. This includes the donor

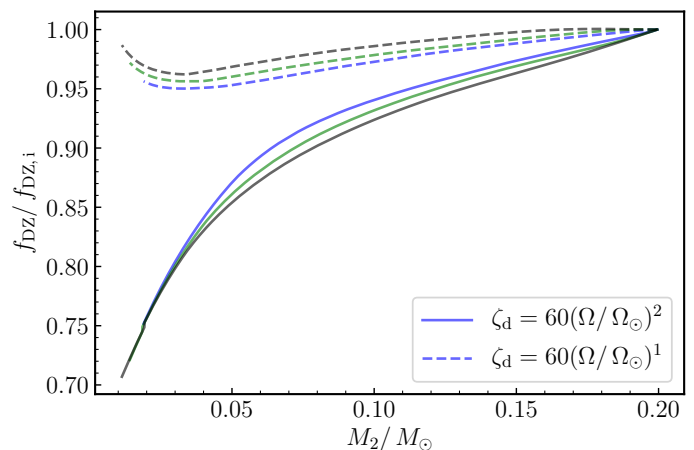


Fig. 4. Evolution of the dead zone relative to that at the beginning of RLOF, $f_{DZ}/f_{DZ,i}$, with M_2 for the models with constant κ . The colours denote the same models as in Figs 1 and C.1, with $\kappa = 0$ shown in blue, $\kappa = 4$ in green, and $\kappa = 15$ in black. The line styles denote the choice of ζ_d . The dead zone for each track was calculated post-evolution using the method of Mestel & Spruit (1987).

stars in CVs. The only difference here is that, owing to tidal locking, P_{orb} governs the behaviour of the dead zone. We calculated the evolution of dead zones using the simple treatment of Mestel & Spruit (1987, their Eqs (8) and (9)), adopting solar parameters for the coronal temperature and mean molecular weight. The choice of these parameters does not alter the qualitative behaviour of our dead zone calculations.

For the expression of the ratio of the magnetic pressure and the thermal pressure at the base of the dead zone, ζ_d , we can study the behaviour of two cases: $\zeta_d = 60(\Omega/\Omega_\odot)$ and $\zeta_d = 60(\Omega/\Omega_\odot)^2$, from Table 1 of Mestel & Spruit (1987). Here, Ω is the orbital angular velocity of the CV. The evolution of the dead zone of the donor star for the models with constant κ in Fig. 1 is shown in Fig. 4. Here, $f_{DZ} = R_2/R_{DZ}$ is the fraction of field lines contributing to MB in the system, where R_{DZ} is the equatorial radius of the dead zone. With no dead zones, $f_{DZ} = 1$. The value $f_{DZ,i}$ denotes the contribution of dead zones at the time of commencement of RLOF.⁶ These tracks demonstrate how the dead zones would behave in a short-period CV. It is seen that when $\zeta_d \propto \Omega$, f_{DZ} changes very little throughout the evolution. However, the dead zones grow (f_{DZ} becomes smaller) with decreasing M_2 when $\zeta_d \propto \Omega^2$, with the drop becoming steep at $M_2 \approx 0.05M_\odot$. A stronger dependence of ζ_d on Ω yields a steeper drop in f_{DZ} . One way in which MB affects dead zones is through the generated magnetic field in the donor (say, by a strong-field dynamo or an α^2 dynamo) that governs the magnetic pressure outside the star (through ζ_d). Dead zones work as an additional mechanism of MB alteration that is always at play regardless of the physical mechanism that drives MB. It can further weaken MB if $d \ln \zeta_d / d \ln \Omega \gtrsim 2$ (Fig. 4).

4. Conclusion

In this Letter, we have shown that the weakening of MB in short-period CVs can help explain the dearth of observed period bouncers. The main idea behind this stems from the fact that to reproduce the correct CV period minimum there ought to

⁶ We note that this plot is made post-evolution so that dead zones do not alter the MB strength of these models.

be some additional AML mechanism below the period gap. This need not necessarily be a constant scaling to GWR, as was employed by Knigge et al. (2011). We introduce an MB at the lower end of the period gap that decreases as the CV approaches its period minimum and find that such a prescription also correctly reproduces the period minimum at about 80 min. In contrast to the systems with constant scaling, these systems spend considerable time around the observed period minimum spike between 80 and 86 min even after they have passed their minimum period. There, they become difficult to distinguish from pre-bounce systems. The mass-transfer rate decreases below the current detection threshold during further evolution driven by GWR and weakening MB.

A direct comparison of our results with observations of the relative fraction of bouncers is difficult because of our ad hoc prescription of MB weakening and an uncertain detection threshold. So, we compare the constant MB models with the weakening MB ones for a range of detection thresholds and find that the latter shows a stronger reduction in the number of observable bouncers. Our models predict that the undetectable bouncers accumulate around $\dot{M}_2 \approx 10^{-12} M_{\odot} \text{ yr}^{-1}$, which can be tested with upcoming surveys that will hopefully reveal low-luminosity bouncers.

The weakening of MB can be caused by physical processes such as a change in the dynamo action in the donor that drives weaker chromospheric activity, the emergence of magnetism in the white dwarf accretor that connects with that of the donor, and thus restricts the outflow of stellar winds, and dead zones in the donor trapping stellar winds. Nevertheless, we admit that the paucity of observed period bouncers may be caused by other selection effects, too, or as-yet-unrecognised physical effects.

Acknowledgements. We thank the referee for a detailed review which greatly improved the paper. AS thanks the Gates Cambridge Trust for his scholarship. AS also thanks Ken Shen and Elmé Breedt for discussions on the nature of short-period CVs. ACR acknowledges support from an NSF Graduate Research Fellowship. AS and ACR are grateful to Franco Giovannelli and the Golden Age of Cataclysmic Variables and Related Objects VI Workshop for facilitating fruitful conversations. SG acknowledges support from the Israel Ministry of Innovation, Science, and Technology (grant No. 1001572596), and from the U.S. – Israel Binational Science Foundation (BSF; grant No. 2022175). AS and SG thank Daniel Blatman for the discussion on the emergence of magnetic fields in white dwarfs. CAT thanks Churchill College for his fellowship.

References

Amantayeva, A., Zharikov, S., Page, K. L., et al. 2021, *ApJ*, 918, 58
 Belloni, D., Schreiber, M. R., Pala, A. F., et al. 2020, *MNRAS*, 491, 5717
 Blatman, D. & Ginzburg, S. 2024, *MNRAS*, 528, 3153
 Chabrier, G. & Küker, M. 2006, *A&A*, 446, 1027
 Galiullin, I., Rodriguez, A. C., Kulkarni, S. R., et al. 2024, *MNRAS*, 528, 676
 Gänsicke, B. T., Dillon, M., Southworth, J., et al. 2009, *MNRAS*, 397, 2170
 Garraffo, C., Drake, J. J., & Cohen, O. 2015, *ApJ*, 813, 40
 Ginzburg, S., Fuller, J., Kawka, A., & Caiazzo, I. 2022, *MNRAS*, 514, 4111–4119
 Goliasch, J. & Nelson, L. 2015, *ApJ*, 809, 80
 Inight, K., Gänsicke, B. T., Breedt, E., et al. 2023a, *MNRAS*, 524, 4867
 Inight, K., Gänsicke, B. T., Schwöpe, A., et al. 2023b, *MNRAS*, 525, 3597
 Isern, J., García-Berro, E., Külebi, B., & Lorén-Aguilar, P. 2017, *ApJ*, 836, L28
 Jermyn, A. S., Bauer, E. B., Schwab, J., et al. 2023, *ApJS*, 265, 15
 Kalomeni, B., Nelson, L., Rappaport, S., et al. 2016, *ApJ*, 833, 83
 Knigge, C. 2006, *MNRAS*, 373, 484
 Knigge, C., Baraffe, I., & Patterson, J. 2011, *ApJS*, 194, 28
 Kolb, U. 1993, *A&A*, 271, 149
 Kollmeier, J. A., Zasowski, G., Rix, H.-W., et al. 2017, *arXiv e-prints*, arXiv:1711.03234
 Li, J. K., Wu, K. W., & Wickramasinghe, D. T. 1994, *MNRAS*, 268, 61
 Littlefair, S. P., Dhillon, V. S., Marsh, T. R., et al. 2008, *MNRAS*, 388, 1582
 Liu, F. K., Meyer, F., Meyer-Hofmeister, E., & Burwitz, V. 2008, *A&A*, 483, 231
 McAllister, M. J., Littlefair, S. P., Dhillon, V. S., et al. 2017, *MNRAS*, 467, 1024

Mestel, L. & Spruit, H. C. 1987, *MNRAS*, 226, 57
 Mohanty, S. & Basri, G. 2003, *ApJ*, 583, 451
 Morin, J., Donati, J. F., Petit, P., et al. 2010, *MNRAS*, 407, 2269
 Morin, J., Dormy, E., Schrunner, M., & Donati, J. F. 2011, *MNRAS*, 418, L133
 Mukai, K. 2017, *PASP*, 129, 062001
 Narayan, R., McClintock, J. E., & Yi, I. 1996, *ApJ*, 457, 821
 Narayan, R. & Popham, R. 1993, *Nature*, 362, 820
 Neustroev, V. V. & Mäntynen, I. 2023, *MNRAS*, 523, 6114
 Paczynski, B. & Sienkiewicz, R. 1981, *ApJ*, 248, L27
 Pala, A. F., Gänsicke, B. T., Belloni, D., et al. 2022, *MNRAS*, 510, 6110
 Pala, A. F., Gänsicke, B. T., Breedt, E., et al. 2020, *MNRAS*, 494, 3799
 Pala, A. F., Schmidtobreick, L., Tappert, C., Gänsicke, B. T., & Mehner, A. 2018, *MNRAS*, 481, 2523
 Paxton, B., Bildsten, L., Dotter, A., et al. 2011, *ApJS*, 192, 3
 Paxton, B., Cantiello, M., Arras, P., et al. 2013, *ApJS*, 208, 4
 Paxton, B., Marchant, P., Schwab, J., et al. 2015, *ApJS*, 220, 15
 Paxton, B., Schwab, J., Bauer, E. B., et al. 2018, *ApJS*, 234, 34
 Paxton, B., Smolec, R., Schwab, J., et al. 2019, *ApJS*, 243, 10
 Predehl, P., Andritschke, R., Arefiev, V., et al. 2021, *A&A*, 647, A1
 Pretorius, M. L., Knigge, C., & Kolb, U. 2007, *MNRAS*, 374, 1495
 Rappaport, S., Verbunt, F., & Joss, P. C. 1983, *ApJ*, 275, 713
 Réville, V., Brun, A. S., Matt, S. P., Strugarek, A., & Pinto, R. F. 2015, *ApJ*, 798, 116
 Sarkar, A. & Tout, C. A. 2022, *MNRAS*, 513, 4169
 Schreiber, M. R., Belloni, D., Gänsicke, B. T., Parsons, S. G., & Zorotovic, M. 2021, *Nature Astronomy*, 5, 648
 Schreiber, M. R., Belloni, D., & van Roestel, J. 2023, *A&A*, 679, L8
 Skumanich, A. 1972, *ApJ*, 171, 565
 Sunyaev, R., Arefiev, V., Babyshkin, V., et al. 2021, *A&A*, 656, A132
 Verbunt, F. & Zwaan, C. 1981, *A&A*, 100, L7
 Warner, B. 2003, *Cataclysmic Variable Stars* (Cambridge University Press)

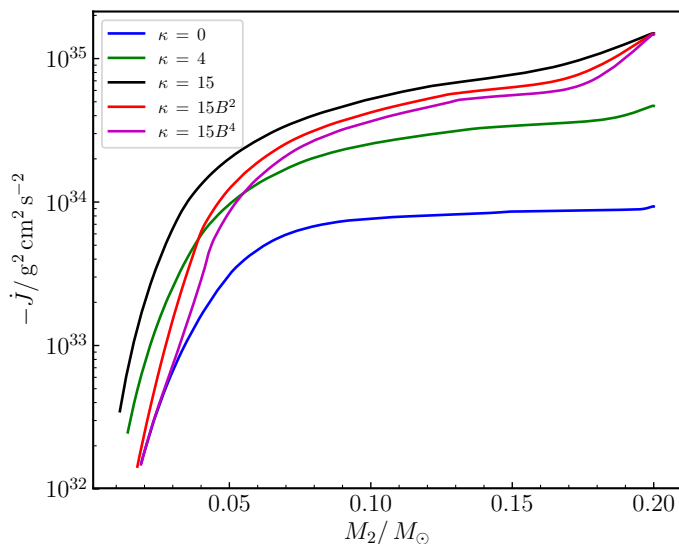


Fig. A.1. Evolution of \dot{J} with M_2 for the models in Fig. 1.

Appendix A: Evolution of angular momentum loss

In Fig. A.1, we plot the evolution of the total AML rate, $\dot{J} \equiv \text{AML}_{\text{GWR}} + \text{AML}_{\text{MB}}$, with the donor mass. We note that although $-\dot{J}$ decreases throughout the evolution for each model, at $M_2 \approx 0.07 M_\odot$ it decreases more steeply for the models in which κ depends on stellar parameters.

Appendix B: A catalogue of period bouncers

We present a catalogue of all known period bouncers in Table B.1. While there are more such candidate systems in the literature (some 25 to 30 in total), we require there to be precise estimates of 1) an orbital period, 2) donor mass, 3) WD mass (and radius), and 4) WD temperature for us to include one in our sample. If a donor mass is not available, we ensure that WD properties are well measured and that there is spectroscopic evidence for a brown dwarf donor. We also indicate the few systems known to be eclipsing because those have, on the whole, more precisely measured donor star parameters.

Appendix C: Computation of \dot{M}_2 and evolution in the $\dot{M}_2 - P_{\text{orb}}$ plane

We computed \dot{M}_2 using the relation derived given in Pala et al. (2022),

$$L_{\text{WD}} = 6 \times 10^{-3} L_\odot \left(\frac{\dot{M}_2}{10^{-10} M_\odot \text{ yr}^{-1}} \right) \left(\frac{M_{\text{WD}}}{0.9 M_\odot} \right)^{0.4} \quad (\text{C.1})$$

which relates the WD mass, radius, and temperature to the accretion rate (Table B.1). It is also possible to estimate accretion rates from the X-ray luminosity or disc luminosity. The former requires a model of the X-ray emission mechanism, and the latter a model of disc geometry. Both require an estimate of accretion efficiency, which is often parametrised as η in the following expression:

$$L = \frac{\eta GM_{\text{WD}} \dot{M}_2}{2 R_{\text{WD}}}, \quad (\text{C.2})$$

where R_{WD} is the WD radius and L is the observed accretion luminosity (either from the disc or from the boundary layer, in

X-rays). However, the range of η in CVs is a subject of current debate (see Sect. 6.1 of Mukai 2017 for a thorough explanation). As an example, one model of accretion is advective dominated accretion flow (ADAF), which was first applied to explain the hard X-ray spectra of CVs in Narayan & Popham (1993). It was later extended in Narayan et al. (1996) to X-ray binaries observed in a low accretion state. In this work, accretion efficiencies have been shown to be very low, with η between 10^{-3} to 10^{-4} . From Eq. (C.2), it is clear how failing to incorporate low efficiencies could lead to an underestimate of the accretion rate, given an observed luminosity. More recently, Liu et al. (2008) applied the ADAF model to X-ray spectra of CVs and found good agreement. Nevertheless, Mukai (2017) warns that a complete analysis of accretion efficiency in CVs, which takes into account interactions between disc annuli, is still needed.

In Fig. C.1, we describe how each model attains $\dot{M}_{2,\text{detect}}$ in the $\dot{M}_2 - P_{\text{orb}}$ plane. The model evolution can be explained as follows. Variation in the MB strength changes the $\dot{M}_2 - R_2$ relation, and consequently the $\dot{M}_2 - P_{\text{orb}}$ relation of a CV, and so a CV attains P_{min} at a larger P_{orb} for a stronger MB (Fig. 1). Now, if MB stays constant post-bounce (say $\kappa = 4$), then as CV bounces P_{orb} increases and \dot{M}_2 decreases. However, for the weakening MB model (say $\kappa = 15B^4$), around the time when the CV bounces, MB becomes negligible. The CV now has to adjust its mass-transfer rate according to the current weak AML strength, but it cannot increase its P_{orb} because the P_{orb} where the CV bounced is too large for its AML strength. \dot{M}_2 has to reduce with little change in P_{orb} . So, the $\kappa = 15B^4$ system essentially stays at approximately 80 min after bouncing before becoming undetectable (when $\dot{M}_{2,\text{detect}} = 10^{-11} M_\odot \text{ yr}^{-1}$). The system stays in the period minimum spike (which is also populated by pre-bounce systems) before becoming undetectable. This is also seen in Fig. 1 (the square in which $\dot{M}_{2,\text{detect}}$ is attained is in the period minimum spike). This track explains observed candidates clustered at the lower end of the period minimum spike in Fig. C.1. Similarly, the track with $\kappa = 15B^2$ bounces at about 86 min but becomes undetectable at about 90 min. This track explains observed candidates clustered at the upper end of the period minimum spike. The system with $\kappa = 4$ emerges from the period minimum spike with $\dot{M}_2 > 10^{-11} M_\odot \text{ yr}^{-1}$. So, if such a constant κ is at play post-bounce, there should be systems populating the region with $86 \leq P_{\text{orb}}/\text{min} \leq 105$ and $\dot{M}_2 \gtrsim 10^{-11} M_\odot \text{ yr}^{-1}$. These are not observed, indicating further that MB weakens post-period minimum. If SRG/eROSITA unveils systems with $\dot{M}_2 \approx 10^{-12} M_\odot \text{ yr}^{-1}$, the $\kappa = 15B^4$ track indicates the existence of a population of systems up to $P_{\text{orb}} \approx 110$ min and the $\kappa = 15B^2$ track up to $P_{\text{orb}} \approx 115$ min. However, because η in Eq. (C.2) is very uncertain and can easily be lower than even 10^{-4} , such low- \dot{M}_2 systems would have very low luminosities. This can make finding them very difficult, even with the newer SRG/eROSITA surveys.

Finally, we note that our accretion rate estimates, based on WD properties (Eq. (C.1)), place the accretion rates of systems such as EZ Lyn (Amantayeva et al. 2021) and SRGeJ0411+6853 (Galiullin et al. 2024) nearly an order of magnitude higher than that reported by authors using X-ray or disc luminosities. Amantayeva et al. (2021) estimated the accretion rate based on the optical disc luminosity, and assumed that $\eta = 1$ in Eq. (C.2) to obtain $\dot{M}_2 \approx 3 \times 10^{-12} M_\odot \text{ yr}^{-1}$ (EZ Lyn* in Fig. C.1). Galiullin et al. (2024) incorporated a bolometric correction to the X-ray luminosity, which assumed a thermal bremsstrahlung model for the emission, to obtain $\dot{M}_2 \approx (1.7 - 7.8) \times 10^{-12} M_\odot \text{ yr}^{-1}$ (SRGeJ0411+6853* in Fig. C.1). However, they did not explore a range of radiative efficiencies. In both cases, the accre-

Table B.1. Known period bouncers with either a well-measured donor mass or accretion rate.

Name	$P_{\text{orb}}/ \text{hr}$	Ecl.?	M_2/ M_{\odot}	M_{WD}/ M_{\odot}	$R_{\text{WD}}/ 0.01 R_{\odot}$	$T_{\text{eff, WD}}/ \text{K}$	$\dot{M}_2/ 10^{-10} M_{\odot} \text{yr}^{-1}$	Ref.
EZ Lyn	1.430	Yes	0.042 ± 0.014	0.85 ± 0.01	0.94	11250 ± 40	$0.242^{+0.003}_{-0.003}$	1
SDSSJ1035 + 0551	1.370	Yes	0.052 ± 0.002	0.94 ± 0.01	0.87 ± 0.01	10100 ± 200	$0.12^{+0.005}_{-0.005}$	2
SDSSJ1057 + 2759	1.510	Yes	0.0436 ± 0.002	0.80 ± 0.015	1.04 ± 0.017	13300 ± 1100	$0.54^{+0.14}_{-0.17}$	3
SDSSJ1433 + 1011	1.300	Yes	0.06 ± 0.003	0.868 ± 0.007	0.958 ± 0.008	12800 ± 200	$0.38^{+0.02}_{-0.02}$	2
SDSS J1501+5501	1.364	Yes	0.053 ± 0.003	0.80 ± 0.03	1.04 ± 0.04	12500 ± 200	$0.426^{+0.009}_{-0.01}$	2
SRGeJ0411+6853	1.625	Yes		0.84 ± 0.07	1.0 ± 0.09	13790 ± 500	$0.56^{+0.04}_{-0.04}$	4
EG Cnc	1.439	No		1.03 ± 0.05	$0.77^{+0.06}_{-0.05}$	12290 ± 55	$0.2^{+0.03}_{-0.03}$	5
GD 552	1.712	No		0.78 ± 0.04	$1.07^{+0.05}_{-0.04}$	10760 ± 40	$0.25^{+0.02}_{-0.03}$	5
1RXS J1050–1404	1.476	No		0.77 ± 0.03	$1.08^{+0.04}_{-0.03}$	11520 ± 50	$0.34^{+0.02}_{-0.03}$	5
QZ Lib	1.539	No		0.82 ± 0.19	$1.01^{+0.23}_{-0.18}$	11420 ± 200	$0.28^{+0.1}_{-0.2}$	5
SDSS J1435+2336	1.300	No		0.84 ± 0.07	$1.0^{+0.08}_{-0.09}$	12000 ± 160	$0.32^{+0.05}_{-0.05}$	5
BW Scl	1.304	No	0.051 ± 0.006	1.007 ± 0.01	$0.8^{+0.014}_{-0.011}$	15145 ± 50	$0.51^{+0.01}_{-0.008}$	5, 6
GW Lib	1.279	No		0.83 ± 0.12	$1.03^{+0.15}_{-0.10}$	16166 ± 350	$1.09^{+0.26}_{-0.34}$	5
WZ Sge	1.360	No		0.80 ± 0.02	$1.05^{+0.03}_{-0.03}$	13190 ± 115	$0.53^{+0.01}_{-0.01}$	5

Notes. The accretion rates are derived from WD mass and temperature estimates (see Eq. C.1). Ecl. stands for eclipsing.

References. (1) Amantayeva et al. (2021); (2) Littlefair et al. (2008); (3) McAllister et al. (2017); (4) Galiullin et al. (2024); (5) Pala et al. (2022); (6) Neustroev & Mäntynen (2023).

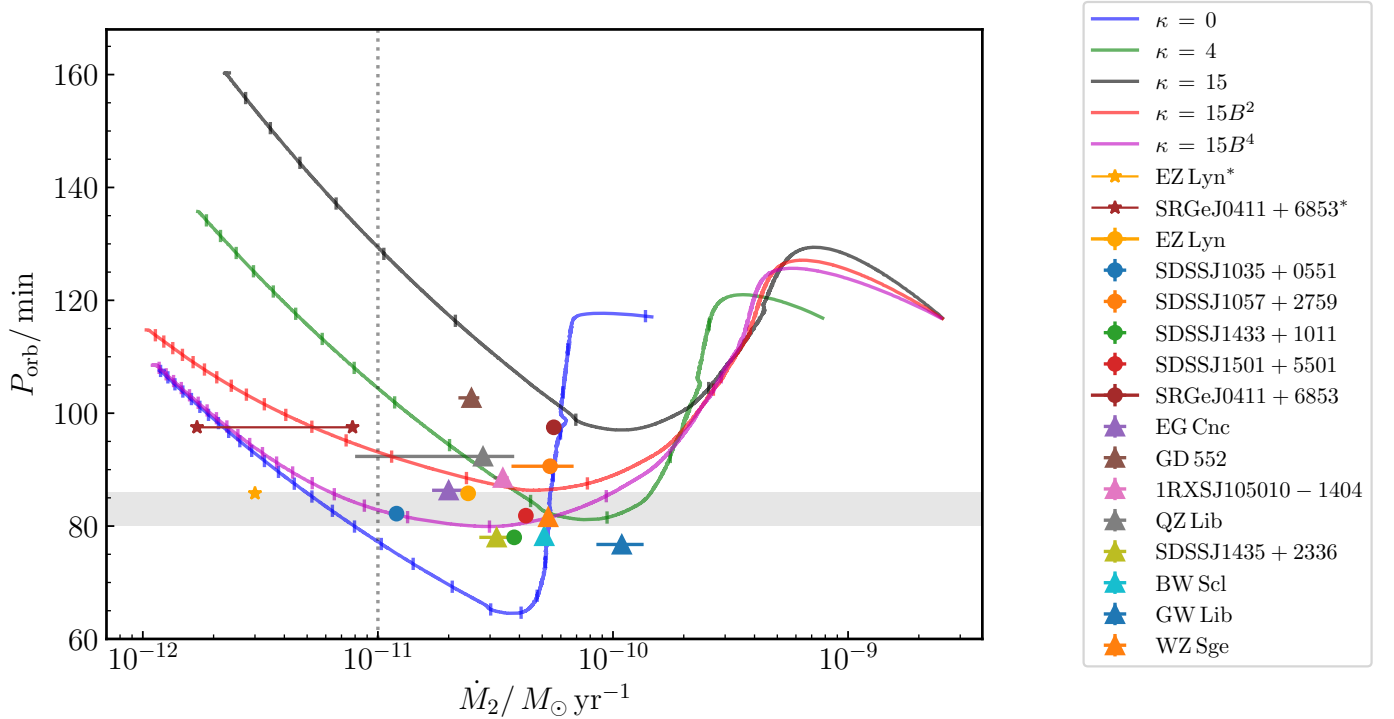


Fig. C.1. Evolution of CVs below the period gap. Solid lines show evolution in the $\dot{M}_2 - P_{\text{orb}}$ plane for the same tracks as in Fig. 1. Ticks on each track denote timesteps of 300 Myr. The dotted vertical line denotes $\dot{M}_2 = 10^{-11} M_{\odot} \text{yr}^{-1}$. During further evolution, the system is presumably undetectable (see text). Observed period bouncer candidates from Table B.1 are also plotted. Eclipsing systems are plotted as circles, while non-eclipsing systems are plotted as triangles. The systems labelled and marked with stars have their \dot{M}_2 derived from X-ray luminosity (Eq. (C.2)), while the others have \dot{M}_2 derived from WD properties (Eq. (C.1)). The horizontal shaded region is the observed period minimum spike ($80 \leq P_{\text{orb}}/ \text{min} \leq 86$) reported by Gänsicke et al. (2009).

tion rates could have been underestimated. Another reason why these may have been underestimated is that \dot{M}_2 (lower end of SRGeJ0411+6853*) is smaller than that for the $\kappa = 0$ model. Assuming that the CV remains semi-detached, the estimates of the $\kappa = 0$ model set the minimum accretion rate post-bounce. Regardless of these uncertainties, the \dot{M}_2 of EZ Lyn* is only a factor of two smaller than that predicted by our $\kappa = 15B^4$ model.

It will agree with our model if we choose $\eta = 0.5$ in Eq. (C.2) to calculate \dot{M}_2 . The \dot{M}_2 of SRGeJ0411+6853* is already in general agreement with both the $\kappa = 15B^2$ and $\kappa = 15B^4$ models. Our model tracks agree well with several systems in Fig. C.1, but notably the $\kappa = 15B^4$ model is in good agreement with all the estimates of SDSSJ1501 and SDSSJ1035 — namely P_{orb} , M_2 , and \dot{M}_2 — while the $\kappa = 15B^2$ model is in agreement with

the P_{orb} and M_2 estimate of EZ Lyn and within a factor of two of its \dot{M}_2 estimate.